

Quantitative description of Josephson-like tunneling in $\nu_T = 1$ quantum Hall bilayers

Timo Hyart^{1,2} and Bernd Rosenow^{1,2}

¹*Max-Planck-Institut für Festkörperforschung, Heisenbergstrasse 1, D-70569 Stuttgart, Germany*

²*Institute for Theoretical Physics, University of Leipzig,
Vor dem Hospitaltore 1, D-04103 Leipzig, Germany*

At total filling factor $\nu_T = 1$, interlayer phase coherence in quantum Hall bilayers can result in a tunneling anomaly resembling the Josephson effect in the presence of strong fluctuations. The most robust experimental signature of this effect is a strong enhancement of the tunneling conductance at small voltages. The height and width of the conductance peak depend strongly on the area and tunneling amplitude of the samples, applied parallel magnetic field and temperature. We find that the tunneling experiments are in quantitative agreement with a theory which treats fluctuations due to meron excitations phenomenologically and takes tunneling into account perturbatively. We also discuss the qualitative changes caused by larger tunneling amplitudes, and provide a possible explanation for recently observed critical currents in counterflow geometry.

I. INTRODUCTION

The existence of a bilayer quantum Hall state at total filling factor $\nu_T = 1$ is well-established both theoretically^{1–26} and experimentally^{27–48}. This state is characterized by remarkable electronic properties such as counterflow superconductivity and a Josephson-like enhancement of tunneling between the two layers.^{1,6–9} Its formation is controlled by the relative magnitude of intra- and interlayer Coulomb interactions, and therefore depends critically on the ratio of interlayer separation d and magnetic length $l_B = \sqrt{\hbar/eB}$. At large d/l_B , there is no quantum Hall effect and the bilayer system behaves qualitatively like two independent composite fermion systems. On the other hand, at small d/l_B , the interlayer Coulomb interaction induces an exotic quantum Hall state, which can be described as an exciton Bose-Einstein condensate or as a pseudospin ferromagnet.^{1,6,7} Here, the pseudospin is formed from the two-valued *which layer* quantum degree of freedom, and condensation occurs because the electrons can lower their interlayer exchange energy by entering a state with uncertain layer index.⁷

Experimentally, the most spectacular effect arising due to the interlayer phase coherence at small d/l_B is a huge enhancement of the tunneling conductance at small voltages. In the incoherent state at large d/l_B , the tunneling in quantum Hall bilayers is strongly suppressed by a Coulomb gap,^{49–52} which is caused by strong electronic correlations and the squeezing of wave functions by the magnetic field rather than by small geometric dimensions.⁵³ Namely, in a strong magnetic field each layer is in a correlated state of its own, and the tunneling event can be considered as an electron suddenly brought from one layer to the other, resulting in an excited state of the system. Relaxation towards the ground state takes place when the energy is carried away by collective excitations, and this excitation energy must be provided by a sufficiently large external voltage.⁵³ On the other hand, if the layers are closer together, the Coulomb gap decreases⁵⁰ due to interlayer correlations⁵⁴, and finally at some critical value of d/l_B a strong and sharp peak ap-

pears in the differential conductance^{28,34}, indicating the transition to an interlayer coherent state with a quantized Hall drag and small counterflow resistances^{30,31,35–38,48}. The coherent state was further characterized by determining the dispersion relation of the collective Goldstone mode²⁹ and the degree of spin polarization^{39,47,48}. Moreover, the phase-transition from incoherent to coherent state^{26,31,33,39,41,42} was studied in some detail.

The Josephson effect with a zero bias supercurrent can be observed when there is a phase difference between two superconductors separated by a tunnel junction. In a quantum Hall bilayer system, the individual layers are not superconducting by themselves, and only the two layers combined can exhibit phase coherence. However, in the coherent state of a clean system with tunnel coupling between the layers, a deviation of the pseudospin orientation from the minimum energy direction is expected to give rise to a zero bias tunnel current between the layers^{8,9}, in analogy to the Josephson current in a superconducting tunnel junction. Experimentally, instead of a zero-bias supercurrent, a Josephson-like enhancement of tunneling^{28,29,32–34,39–46} at small interlayer bias voltage was observed. A significant amount of theoretical effort has been devoted to understanding the finite height and width of the conductance peak of this Josephson-like tunneling at small voltages^{10–15,17,18,23} as well as the magnitude of the critical tunneling current^{21,24,25}. These approaches differ in how the bias voltage, quasiparticles and disorder are introduced into the theory. In one type of approach^{18,21,23}, the clean limit without charge disorder is considered. Then, the critical current is given by the maximum current at which the order parameter can be static, and the tunneling conductance cannot be described in terms of condensate dynamics alone, because it also depends on the fermionic quasiparticles which transport the charge between leads and bulk.^{18,23}

Experimentally investigated samples are probably not in the clean limit, and experimental results indicate that disorder-induced topological defects, so-called merons, are important.^{10–12,14–16,19,20,22,24,25} Merons carry a charge $\pm e/2$ and are characterized by their vorticity and the layer in which the charge resides.^{1,2,7,10} Be-

cause merons are nucleated by charge disorder, they exist also at low temperatures, and their dynamics is expected to give rise to dissipation and to strongly affect the interlayer tunneling.^{10–12,14–16,19,20,22,24} Merons can be taken into account in the description of Josephson-like tunneling by introducing a phenomenological vortex field.^{10–12,24,25} Both dynamic^{10,11} and static^{12,24,25} vortex fields have been considered in the literature. Despite similar starting points, static and dynamic approaches predict different characteristic features for the tunneling current.

Spatial fluctuations in the vortex field are accounted for by a correlation length ξ , which governs the decay of the pseudospin ferromagnetic order. Spatial fluctuations are caused by the formation of compressible puddles, which are thought to arise due to local fluctuations in the density of dopants. If the local density of merons created by charge disorder is sufficiently high, the merons can screen the random potential and delocalize. As merons are vortices of the order parameter field, spatial correlations in the order will decay on the typical distance between puddles, which in turn is determined by the set-back distance to the dopant layer, such that one expects $\xi \sim 100 - 200 \text{ nm}$ ^{10,20}.

In the present manuscript, we study the influence of a dynamical vortex field on interlayer tunneling deep inside the coherent phase. Dynamical fluctuations of the order parameter are caused by the dynamics of merons in this picture. At temperatures lower than the energy gap but still comparable to it, one can imagine that thermally activated hopping of merons from one puddle to another is the dominant source of fluctuations. By mapping the quantum Hall bilayer to a classical two-dimensional XY model with a symmetry-breaking field and with disorder, Fertig and Straley¹⁴ have found that disorder nucleates strings of overturned spins, which connect vortices and antivortices at their ends. At low temperatures, this state shows glassy features and gives rise to anomalously large fluctuations of the vortex field. The temperature dependence of interlayer tunneling in a coherence network of puddles and ordered regions was analyzed in Ref. 15.

We model dynamical vortex field fluctuations by introducing an exponential time decay of local pseudospin correlations^{10,11}, which is governed by a correlation time τ_φ . In this approach, tunneling between the two layers can be treated perturbatively, and Josephson oscillations in the presence of vortex field fluctuations give rise to the finite tunneling peak observed in the experiments. This effect strongly resembles the Josephson tunneling in small Josephson junctions in the presence of thermal or quantum fluctuations^{55–57}. We find that the current-voltage (I-V) characteristic of interlayer tunneling is characterized by a voltage scale

$$V_0 = \hbar u / e \xi \quad (1)$$

and by the scale for the maximum tunnel current

$$I_0 \propto \frac{e \xi^2 L^2}{\hbar \rho_s} \frac{\Delta_{SAS}^2}{l_B^4} . \quad (2)$$

Here, u is the velocity of the pseudospin wave mode, Δ_{SAS} is the tunnel coupling between the two layers, L^2 is the area of the sample and ρ_s is the pseudospin stiffness. The functional form of the I-V characteristic is controlled by the temperature dependent decoherence rate

$$\alpha(T) = \frac{\xi}{u \tau_\varphi(T)} , \quad (3)$$

which for instance enters into the zero bias conductance. For small values of α we obtain

$$G_0(T) = \frac{I_0}{V_0} \frac{2}{\alpha(T)} . \quad (4)$$

While the zero bias conductance increases when $\alpha \rightarrow 0$, the maximum tunnel current saturates in this limit to a value πI_0 . An in-plane magnetic field suppresses the conductance peak, and we find that the characteristic field scale for this suppression is $\Phi_0 / (d \xi)$, where $\Phi_0 = h/e$ is the flux quantum.

We compare our theoretical predictions to the experimentally observed dependencies of the tunneling current on sample area, tunneling amplitude, applied parallel magnetic field and temperature. We find that experimental results and theoretical predictions are in excellent agreement. Despite the comparatively large number of parameters in our theory, we find that all parameters can be determined uniquely from experimental data and that the parameter values obtained in this way are in very good agreement with theoretical estimates. We find that the apparent temperature dependence of the tunneling conductance³⁴ $G_0 \propto \exp(-T/T_0)$ can be explained as a crossover between an activated and a power law temperature dependence of $\alpha(T)$, which in turn has a natural explanation in terms of vortex field fluctuations.

More recently^{43–46}, intriguing observations were made in bilayer samples with larger tunneling amplitude. In particular, jumps of the tunnel current were observed and described in terms of critical tunnel currents about two orders of magnitude larger than in previous experiments. We find that these observations can still be explained in the framework of a perturbative approach^{10,11} when taking into account that the tunneling resistance between the layers is so small in these samples that the other resistances in the system, such as circuit, contact, longitudinal and Hall resistances, become important. Our approach also provides an explanation for recently observed critical currents in a counterflow geometry⁴⁶. This surprisingly good agreement with the experiments over a wide range of tunneling amplitudes raises questions regarding the region of validity of the perturbative treatment of the tunneling. We give a short discussion of this important theoretical issue in Section VI.

Our paper is organized as follows. In Section II we describe the theory of interlayer tunneling in the presence of fluctuations caused by the meron excitations. In Section III we compare the experimental tunneling I-V characteristic obtained using samples with extremely small tunneling amplitude to our theoretical predictions. We find a

good quantitative agreement between theory and experiments. In Section IV we apply the theory to describe the qualitative changes observed in recent experiments where the tunneling amplitude of the samples was significantly larger. In Section V, we compare with previous theoretical approaches, and finally in Section VI we give a summary of our findings and discuss the limits of the validity of our approach.

II. THEORY OF INTERLAYER TUNNELING IN THE PRESENCE OF MERON EXCITATIONS

We concentrate on the tunneling deep inside the coherent phase at $\nu_T = n_0 \hbar / (eB) = 1$, where $n_0 = (2\pi l_B^2)^{-1}$ is the average density. We assume that the real spin is fully polarized in agreement with the experiments^{39,47,48}. The pseudospin is therefore the most relevant degree of freedom in our problem: The low-energy excitations of the system are the pseudospin waves and the merons. The theoretical analysis presented in this section largely follows that of Stern et al. in Ref. 10. In the absence of tunneling, the pseudospin waves are described by a Hamiltonian density^{1,7,10}

$$\mathcal{H} = \frac{1}{2} \rho_s (\nabla \varphi)^2 + \frac{(en_0 m_z / 2)^2}{2\Gamma}, \quad (5)$$

where $\vec{m} = (\cos \varphi, \sin \varphi, m_z)$ is the pseudospin vector, ρ_s is the pseudospin stiffness and Γ is the capacitance per area. The momentum conjugate to φ is $\pi = \hbar n_0 m_z / 2$. Physically the first term in equation (5) arises from the loss of optimal Coulomb exchange energy: If the pseudospin varies in space, the spatial part of the many-particle wave function cannot be fully antisymmetric. The second term measures the capacitive energy. Because of exchange effects between the layers Γ is expected to be strongly enhanced from its electrostatic value.^{7,10,21} The dispersion relation for collective pseudospin waves (Goldstone mode) is

$$\omega_{\vec{k}} = uk, \quad (6)$$

where the velocity of the pseudospin waves u is

$$u = \sqrt{\frac{\rho_s}{\Gamma}} \frac{e}{\hbar}. \quad (7)$$

The tunneling energy should be included in the Hamiltonian (5) as $T_+ + T_-$ ^{1,7,10}, where the tunneling operators are

$$T_{\pm} = -\lambda \int d^2 r e^{\pm i\varphi} e^{\pm i\varphi_m} e^{\pm ieVt/\hbar} e^{\pm iQ_B x}. \quad (8)$$

Here $\lambda = \Delta_{SAS} / (8\pi l_B^2)$, $Q_B = eB_{\parallel} d / \hbar$, B_{\parallel} is the in-plane magnetic field and V is the interlayer voltage, which we assume to be constant in space. The merons are included phenomenologically with the help of the vortex field φ_m .^{10-12,24} Using the commutation relation for

φ and π it is easy to verify that the tunneling operators T_{\pm} change the charge on the capacitor plates by $\pm e$.

Both counterflow and tunneling experiments suggest that at least part of the merons are mobile. Therefore, we assume that the vortex field is dynamic. The tunneling current depends on the details of vortex field dynamics, which we assume to be characterized by a correlation length ξ and a correlation time τ_{φ} . For the correlation function we make the specific assumption

$$\langle e^{i\varphi_m(\vec{r},t)} e^{-i\varphi_m(\vec{0},0)} \rangle = e^{-r/\xi} e^{-|t|/\tau_{\varphi}}, \quad (9)$$

which appears to produce a good agreement between theory and experimental results. By studying the experimentally found dependence of the tunneling current on a parallel magnetic field, we find strong evidence that $\xi \sim 100 - 200$ nm, in agreement with earlier theoretical estimates^{10,20}. Because pseudospin fluctuations are uncorrelated on scales much larger than ξ , we can at least qualitatively think of the small domains of size ξ^2 as individual Josephson junctions. These small domains are well-coupled to each other by counterflow and transport currents. We assume that the tunneling can be considered perturbatively due to the reasonably small correlation time τ_{φ} caused by the strong fluctuations of the vortex field¹⁰. The validity of the perturbative treatment of the tunneling has been well-established⁵⁶ in small Josephson junctions in the presence of fluctuations, but the justification of similar assumption in quantum Hall bilayers is questionable especially at low voltages^{11,12} essentially because the phase φ describes both the counterflow currents and the tunneling simultaneously. Nevertheless, we find that the perturbative treatment of the tunneling gives a good quantitative description of the Josephson-like tunneling for all voltages and a surprisingly large range of tunneling amplitudes. We discuss this unexpected result and the limits of validity of our approach in more detail in Section VI. In this section we concentrate on a situation where the tunneling resistance is larger than the intralayer resistances, R_{xx} and R_{xy} , so that the interlayer voltage can be considered homogeneous. However, we stress that our approach can easily be extended to a case where the interlayer voltage varies slowly in space. We believe that the interlayer voltage is very homogeneous in the experiments where the tunneling amplitude is small^{28,29,32-34,39-42}. In the case of larger tunneling amplitudes the inhomogeneities will affect the details of the tunneling I-V characteristics, but we believe that they still do not play an important role in the main qualitative features observed in the experiments reported in Refs. 43-46 (see Section IV).

The I-V characteristics can now be calculated using Eqs. (5)-(8) and Fermi's golden rule, similar to the case of Josephson junctions^{56,58}. The result of this calculation is

$$I(V, B_{\parallel}) = \frac{4e\lambda^2 L^2}{\hbar^2} \int_0^{\infty} dt \int d^2 r G_m(r, t) e^{-D(r,t)/2} \times \sin \frac{C(r,t)}{2} \cos(Q_B x) \sin \frac{eVt}{\hbar}, \quad (10)$$

where

$$D(r, t) = \sum_{\vec{k}} \frac{\hbar u}{L^2 \rho_s k} [1 - \cos(\vec{k} \cdot \vec{r}) \cos(ukt)] \coth \frac{\beta \hbar u k}{2}, \quad (11)$$

$$\begin{aligned} C(r, t) &= \sum_{\vec{k}} \frac{\hbar u}{L^2 \rho_s k} \sin(ukt) \cos(\vec{k} \cdot \vec{r}) \\ &= \frac{\hbar}{2\pi \rho_s} \theta(ut - r) \left[t^2 - \frac{r^2}{u^2} \right]^{-1/2}, \quad (12) \end{aligned}$$

$\beta = 1/k_B T$ and $G_m(r, t) = \langle e^{i\varphi_m(\vec{r}, t)} e^{-i\varphi_m(\vec{0}, 0)} \rangle$ is the correlation function for φ_m . This result has been found previously in Ref. 10, but for completeness we give a detailed derivation of equations (10)-(12) in Appendix A.

In order to calculate D , we need to define an ‘‘ultraviolet cut-off momentum’’¹⁰ $k_0 = \kappa\sqrt{2}/l_B$, where it is expected that $\kappa \approx 1$. Although some of the parameters, like ρ_s , Γ and Δ_{SAS} , can be theoretically estimated^{7,10,21}, there remain reasonably large uncertainties in their actual values. We find that it is possible to determine most of the parameters based on experimental data and the obtained values are in good agreement with the theoretical predictions. Before comparing theory with experiments, we will make certain simplifying assumptions. The theoretically estimated value for pseudospin stiffness is $\rho_s \sim 0.4 \text{ K}^{10}$, and according to Ref. 23 this parameter is likely to be the most reliably known continuum model parameter. Using this value of ρ_s and the values of the other parameters found below, we have numerically checked that D depends only weakly on temperature in the experimentally relevant temperature range. Therefore, we can use everywhere the zero temperature value

$$D_0 \approx \frac{\hbar u k_0}{2\pi \rho_s} = \kappa \sqrt{\frac{e^3 B}{2\pi^2 \rho_s \Gamma \hbar}}. \quad (13)$$

For $B = 2 \text{ T}$, we obtain $D_0 \sim 3.3$, but an accurate estimate is not possible due to the uncertainty related to the ultraviolet cut-off momentum. With similar assumptions, we have numerically checked that we can use the following first order expansion in Eq. (10)

$$\sin \frac{C(r, t)}{2} \approx \frac{C(r, t)}{2}. \quad (14)$$

These simplifications were justified also in Ref. 10.

By using the Eqs. (10)-(9) and the approximations outlined above, we get ($R = r/\xi$ and $q = k\xi$)

$$\begin{aligned} I &= I_0 \int dq \left[\frac{\alpha}{\alpha^2 + (V/V_0 - q)^2} - \frac{\alpha}{\alpha^2 + (V/V_0 + q)^2} \right] \\ &\quad \times \int dR R e^{-R} J_0(qR) J_0(Q_B \xi R), \quad (15) \end{aligned}$$

where

$$I_0 = \frac{e}{\hbar} \frac{\xi^2 L^2}{\rho_s} \frac{\Delta_{SAS}^2}{l_B^4} \frac{e^{-D_0/2}}{64\pi^2}, \quad (16)$$

and V_0 and α are given by Eqs. (1) and (3), respectively. In Appendix B we give an alternative derivation of Eq. (15) where the quantum fluctuations are neglected. Similarly as in Ref. 12, we solve the Sine-Gordon equation perturbatively, but in contrast to Ref. 12 we also take into account the dynamics of the vortex field. Finally, we obtain the same expression (15) for the I-V characteristics except that now the factor $e^{-D_0/2}$ does not appear in the equation for I_0 . We interpret this factor as the effect caused by quantum fluctuations.

In the absence of a magnetic field, $Q_B = 0$, we obtain

$$I(V) = I_0 \int dq \left[\frac{\alpha}{\alpha^2 + (V/V_0 - q)^2} - \frac{\alpha}{\alpha^2 + (V/V_0 + q)^2} \right] \frac{1}{(1 + q^2)^{3/2}}. \quad (17)$$

In the limit $V \rightarrow 0$ and for small values of α , the peak conductance $G_0 = \left. \frac{dI}{dV} \right|_{V=0}$ is given by Eq. (4). The maximum tunneling current in the limit $\alpha \rightarrow 0$ saturates to a value πI_0 .

We expect that V_0 , I_0 and ξ depend only weakly on temperature. The strong temperature dependence observed in experiments would then be caused by the temperature dependence of τ_φ . In our opinion, this assumption is in agreement with more detailed theoretical models where the meron dynamics were analyzed^{14,15,19}. We expect that for temperatures comparable to the thermal activation gap Δ_g , the temperature dependence of τ_φ arises mainly due to thermally activated hopping of the merons. On the other hand, the temperature dependence of τ_φ at temperatures much smaller than Δ_g could originate from glassy excitations of the pinned meron system, which were predicted¹⁴ to act as a dissipative environment.

The determination of the different theoretical parameters of the model is discussed in detail in Section III. We summarize the methods used to determine them and the values we obtain in table I. The values of the parameters obtained using the experimental data are in good agreement with the theoretical expectations^{7,10,20,21}.

III. QUANTITATIVE DESCRIPTION OF JOSEPHSON-LIKE TUNNELING IN THE CASE OF SMALL Δ_{SAS}

We start by considering the first experimental observations of the Josephson-like tunneling^{28,29,32,34}. Our theory should be most applicable to these experiments, because the tunneling amplitudes of the samples were extremely small, and therefore higher order tunneling processes can be safely neglected. In addition, the tunneling resistance is larger than the intralayer resistances R_{xx} and R_{xy} , so that the interlayer voltage can be considered to be constant in space. We expect that in samples with sufficiently small Δ_{SAS} tunneling is a bulk phenomena which takes place homogeneously throughout the whole

Parameter	Method of determination	Value
ρ_s	Theoretical estimate	~ 0.4 K
ξ	Dependence of the tunneling conductance on B_{\parallel}	~ 130 nm
u	Resonant enhancement of the current at $eV = \hbar u Q_B$	~ 14 km/s
Γ	Using estimates for ρ_s and u	$\sim 10\epsilon\epsilon_0/d$
τ_φ	Height and width of the conductance peak	Temperature dependent
Δ_{SAS}	Tunneling I-V characteristics at $\mathbf{B} = 0$	~ 10 μ K ~ 100 μ K

TABLE I: Determination of the parameters. The different estimates for $\Delta_{SAS} \sim 10$ μ K and $\Delta_{SAS} \sim 100$ μ K correspond to samples considered in Sections III and IV, respectively.

sample area, independent of the sample geometry. Recently, it was found⁴⁰ that the peak in the tunneling conductance is proportional to the area of the sample. Moreover, it seems that in these experiments the tunneling current at all voltages scales proportionally to the area. These observations are explained naturally within the present approach, which predicts the current scale I_0 to be proportional to the area [see Eq. (16)].

The layer separation and the surface area in these experiments^{28,29,32,34} are $d = 27.9$ nm and $L^2 = 250 \cdot 250$ μm^2 , respectively. The tunneling amplitude can be determined³⁴ by solving the Schrödinger equation for the specific structure. Another possibility is to use the reasonably well-understood^{52,59} I-V characteristics at $B = 0$ as explained in Ref. 34. These two methods are in good agreement with each other³⁴, and therefore we are reasonably confident that Δ_{SAS} in these experiments is approximately 5 – 10 μ K. We discuss the experimental and theoretical estimates for the other parameters ξ , τ_φ and u below.

A. Dependence on parallel magnetic field

The in-plane magnetic field in quantum Hall bilayers has two main effects on the Josephson-like tunneling. It suppresses the small-bias current and results in resonant enhancements of the tunneling current at voltages satisfying $eV = \hbar u Q_B$ (see Fig. 1). In this section we discuss the physics behind these effects and determine the values of ξ and u by comparing the theory and experiments. We concentrate on the low voltage part of the I-V characteristics where the experimentally measured [Fig. 1 (a)] and theoretically calculated [Fig. 1 (b)] tunneling currents are in good agreement with each other. The theoretically calculated tunneling currents at large voltages are typically significantly smaller than the experimentally measured currents [cf. Figs. 1 (a) and (b)]. The origin of this discrepancy is probably an incoherent contribution to tunneling discussed in more detail in

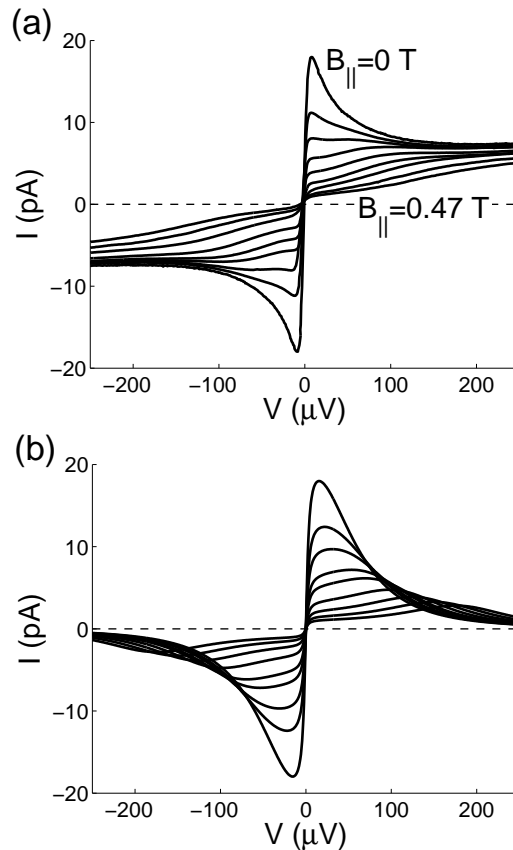


FIG. 1: (a) Measured I-V characteristics for $d/l_B = 1.61$, $T = 25$ mK and different values of parallel magnetic field $B_{\parallel} = 0, 0.11, 0.15, 0.20, 0.23, 0.29, 0.35, 0.41, 0.47$ T. (b) Theoretical I-V characteristics obtained using Eq. (15) for $V_0 = 73$ μ V, $I_0 = 7.1$ pA, $\alpha = 0.04$, $\xi = 126$ nm and the same values of parallel magnetic field. The determination of the theoretical parameters is described in the text. The experimental curves are reproduced from the experimental data provided by I. B. Spielman *et al.* and reported in Ref. 34.

Section VI.

As already pointed out the domains of size $\sim \xi^2$ can, at least qualitatively, be considered as individual Josephson junctions, which are well-coupled to each other by counterflow and transport currents. If a magnetic flux Φ is applied across a Josephson junction, it tries to induce a circulating current inside the junction.⁶⁰ Due to this effect, the critical tunneling current of the Josephson junction oscillates as a function of Φ/Φ_0 , where Φ_0 is the magnetic flux quantum. The current completely vanishes if an integer number of flux quanta is applied across the junction and the dependence, in general, is typically referred to as Fraunhofer diffraction pattern by the analogy with the case of light passing through a narrow rectangular slit.⁶⁰ Based on our analogy, we can now define for each domain a magnetic flux penetrating the area between the layers as $\Phi = B_{\parallel}\xi d$. Similarly to the case of Josephson junctions, we expect that the current vanishes quickly as a function of Φ/Φ_0 . The important difference

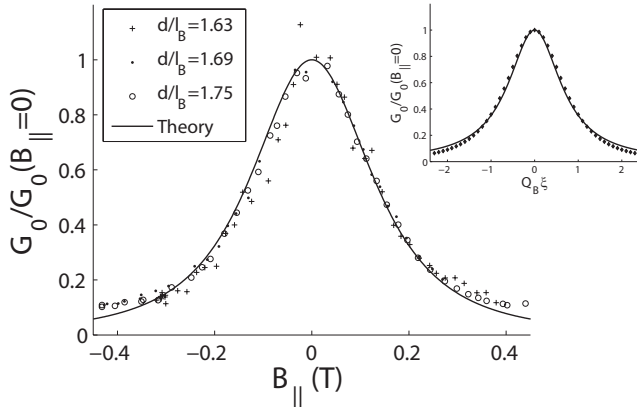


FIG. 2: Experimentally measured and theoretically calculated small bias tunneling conductance as a function of parallel magnetic field B_{\parallel} . The experimental results were obtained at $T = 25$ mK. The small-bias tunneling conductance was calculated using Eq. (15) for $\alpha = 0.04$ and $\xi = 126$ nm. The value of ξ was obtained by fitting Lorentzians to the theoretical and experimental results and by setting the widths of the Lorentzians equal to each other. Inset shows the theoretical small bias conductance as a function of $Q_B\xi$ (dots) and the corresponding Lorentzian fit (line). The experimental data was provided by I. B. Spielman *et al.* and has been reported in Ref. 34.

to standard Josephson junctions is that in our case, the size of the junctions is not well-defined and therefore the Fraunhofer diffraction pattern is "washed away". Here the exact form of the r dependence of the vortex-field correlation function $G_m(r, t)$ also becomes important. It defines the size distribution of our Josephson junctions and therefore it strongly affects the shape of the small-bias tunneling conductance plotted as a function of B_{\parallel} . We find that the exponential dependence given by Eq. (9) gives significantly better agreement with the experiments than the Gaussian dependence suggested in Ref. 10.

Figure 2 shows the experimentally measured small bias tunneling conductance as a function of B_{\parallel} and the corresponding theoretical result obtained using Eq. (15). Both dependencies are approximately Lorentzian as demonstrated for the theoretical curve in the inset of Fig. 2. The half width at half maximum (HWHM) of the Lorentzians fitted to the experimental and theoretical curves are $B_{\parallel}^{\text{HWHM}} \approx 0.138$ and $Q_B^{\text{HWHM}}\xi \approx 0.735$. Using the relation $Q_B = eB_{\parallel}d/\hbar$, we find $\xi \approx 126$ nm. This method of determining ξ is extremely robust against variation of the other theoretical parameters. The obtained value is completely independent of the values of I_0 and V_0 , and it changes only by a few percent if the parameter α is varied between 0.001 and 0.1. Moreover, the value of ξ obtained in this way is in excellent agreement with the theoretical expectations in Refs. 10,20,24. It is also important to note that in clean samples a Fraunhofer pattern has been predicted⁹, and much smaller magnetic fields will induce circulating tunneling currents. Therefore, the in-

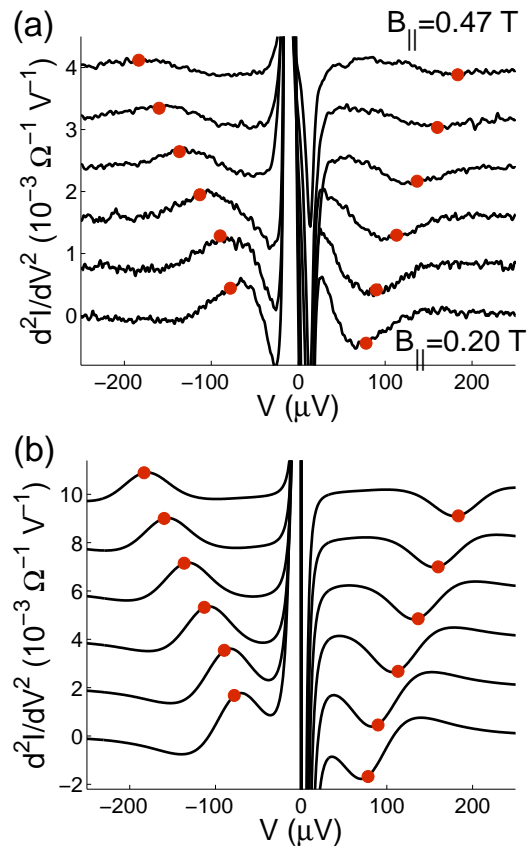


FIG. 3: (color online). (a) Experimental measurement of d^2I/dV^2 for different values of parallel magnetic field $B_{\parallel} = 0.20, 0.23, 0.29, 0.35, 0.41, 0.47$ T. (b) Theoretical curves obtained using $V_0 = 73$ μV , $I_0 = 7.1$ pA, $\alpha = 0.04$, $\xi = 126$ nm and same values of B_{\parallel} . Dots show the expected locations of the resonances $V^* = \hbar u Q_B/e$, which for sufficiently large Q_B are very close to the local extrema of d^2I/dV^2 . In theoretical curves we have introduced larger offset ($2 \cdot 10^{-3} \Omega^{-1} V^{-1}$) between the curves than in experimental results ($0.8 \cdot 10^{-3} \Omega^{-1} V^{-1}$). The experimental curves are reproduced from the experimental data provided by I. B. Spielman *et al.* and reported in Ref. 34.

plane magnetic field dependence of the small-bias tunneling conductance clearly manifests the important role of the merons in the Josephson-like tunneling.

The second interesting effect caused by the in-plane magnetic field are the additional enhancements of the tunneling current at voltages $V^*(B_{\parallel})$ satisfying $eV^* = \hbar u Q_B$. The origin of these resonances is nicely explained in Refs. 10–12. The parallel magnetic field allows only tunneling between states that differ by a momentum Q_B , and energy conservation requires that the energy of these states differs by eV . In the absence of a dissipative environment, there would be just a single linearly dispersing collective mode $\omega_{\vec{k}} = uk$ and therefore both conditions can be satisfied only if the voltage satisfies the resonance condition $eV^* = \hbar u Q_B$. Therefore the resonant enhancements of the tunneling current in the I-V characteristic essentially map the dispersion relation of the

pseudospin waves.^{10–12} Because of the finite correlation length and time caused by the merons, these resonances are not sharp but they can still be clearly seen both in the experimental and theoretical curves by plotting the second derivative d^2I/dV^2 as a function of V as shown in Fig. 3. The second derivative is not sensitive to any linear background conductance and therefore it shows more clearly the nonlinear features in the I-V characteristics. In particular the voltages V^* at the resonances can be determined by finding the extrema of d^2I/dV^2 , which indicate a maximum of the curvature of the I-V characteristic. This result was already anticipated in Refs. 29 and 34, where the velocity u of the pseudospin waves was obtained experimentally by determining for each magnetic field B_{\parallel} the voltage V^* where d^2I/dV^2 has an extremum, and by fitting a linear relation $V^* = \hbar u Q_B / e$ to the data points. We have theoretically confirmed the validity of this approach by numerically determining the locations V^* of extrema of d^2I/dV^2 for different values of Q_B . For $Q_B \xi \gtrsim 2$, the numerically determined function $V^*(Q_B)$ can be approximated by the linear relation $V^* = \hbar u Q_B / e$ within an accuracy of few percents. In addition, the numerically determined function $V^*(Q_B)$ is completely independent of I_0 and practically independent of α , i.e. it does not change within our numerical accuracy when α is varied between 0.001 and 0.1. Therefore, the experimentally found velocity $u \approx 14$ km/s can be considered as a reliable estimate of the actual velocity of pseudospin waves. This value of u is somewhat smaller than theoretically expected^{7,10,21,29,34}, but probably still within the theoretical uncertainties because the parameters ρ_s and Γ are not known accurately.

By using our estimates for the correlation length ξ and Goldstone mode velocity u , we find $V_0 \approx 73$ μV , which yields good agreement between theoretical and experimental curves in Figs. 1 and 3. We can now determine the parameters α and I_0 by using the measured values of small-bias tunneling conductance $G_0 = 4.68 \cdot 10^{-6} \Omega^{-1}$ and maximum tunneling current $I_{\max} = 18$ pA at $B_{\parallel} = 0$. We obtain $\alpha \approx 0.04$ and $I_0 \approx 7.1$ pA. By assuming that $\rho_s \approx 0.4$ K, we estimate using Eq. (16) that $I_0 \sim 4 - 16$ pA (corresponding to $\Delta_{SAS} = 5 - 10$ μK and $d/l_B = 1.6$). Therefore the values of the parameters V_0 , I_0 and ξ determined by fitting the theory to the experimental data shown in Figs. 1, 2 and 3 are consistent with Eq. (16). Moreover, we find that the exchange enhanced capacitance Γ is more than 10 times larger than the electrostatic value. This means that an interlayer bias $V \sim 100$ μV can cause a density imbalance of 5%. We believe that the density imbalance induced by the interlayer voltage plays an important role in the recent tunneling experiments performed in the counterflow geometry (see Section IV).

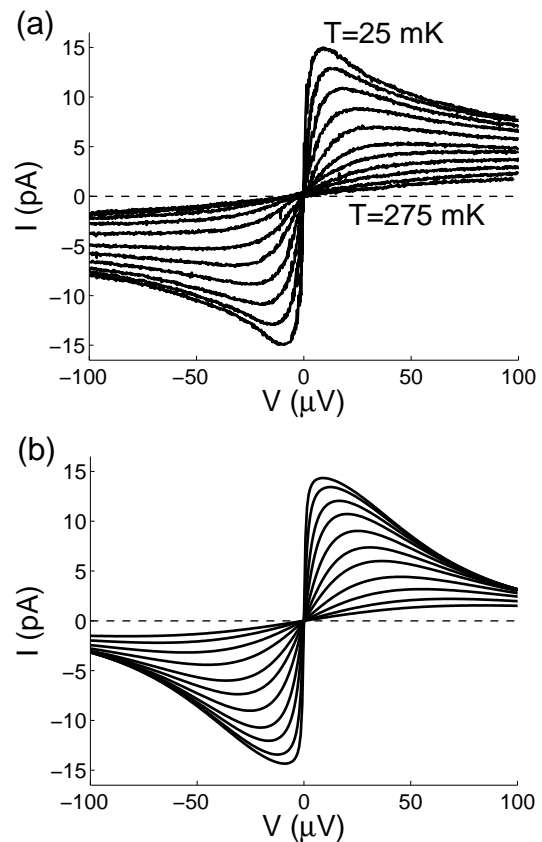


FIG. 4: (a) Experimentally measured I-V characteristics at $d/l_B = 1.50$ and different temperatures $T = 25, 50, 75, 100, 125, 150, 175, 200, 225, 250, 275$ mK. (b) I-V characteristics obtained using Eq. (17) for $V_0 = 73$ μV , $I_0 = 4.9$ pA and different values of α , which are fitted at each temperature. The obtained temperature dependence of α is shown in Fig. 6. The experimental curves are reproduced from the experimental data provided by I. B. Spielman *et al.* and reported in Ref. 34.

B. Temperature dependence

The measured temperature dependence of the I-V characteristic is shown in Fig. 4 (a). Plotted on a single logarithmic scale, the temperature dependence of the peak conductance seems to be consistent with $G_0 \propto \exp(-T/T_0)$ as pointed out in Ref. 34 (see Fig. 5). Such a temperature dependence is not expected because it differs significantly from the temperature dependence of the tunneling current in standard Josephson junctions^{55,57}, and it seems naively that the small-bias tunneling conductance would stay finite even at zero temperature³⁴ in contrast to theoretical expectations^{10–12}.

We argue that the experimentally observed temperature-dependence of the I-V characteristic can be described using the parametrization of our theory. Based on the in-plane magnetic field dependencies of the small-signal tunneling conductance measured at different temperatures³⁴, we can estimate that ξ depends

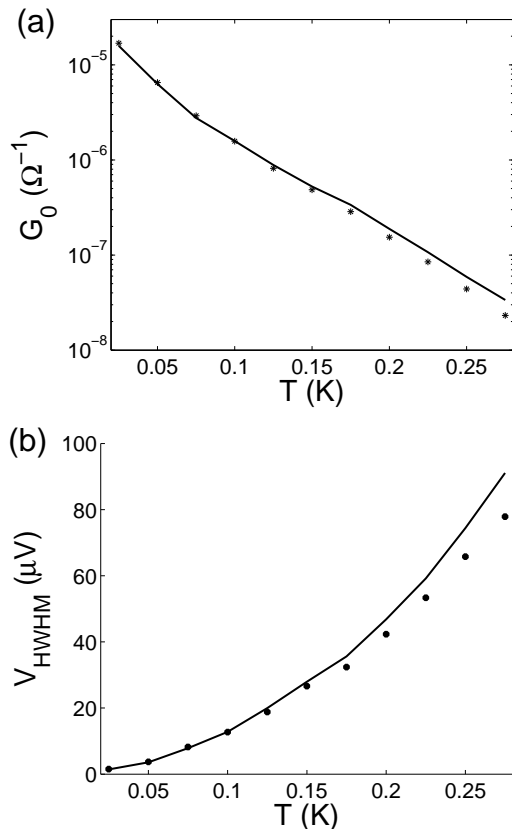


FIG. 5: Temperature dependencies of (a) the height and (b) the width of the conductance peak. Dots show the experimental measurements and the lines show the theoretical values obtained using $V_0 = 73 \mu\text{V}$, $I_0 = 4.9 \text{ pA}$ and the temperature dependence of α shown in Fig. 6. The experimental data was provided by I. B. Spielman *et al.* and has been reported in Ref. 34.

only weakly on temperature. Moreover, we expect that ρ_s and Γ do not depend strongly on temperature at the experimentally relevant temperatures deep inside the coherent phase. This assumption could be tested by measuring the temperature dependence of u . Therefore, we assume that the main temperature dependence of the tunneling current must originate from the temperature dependence of τ_φ . Since the tunneling current according to Eq. (17) depends on τ_φ only through the parameter α , we will use α as the fitting parameter.

Fig. 4 (b) shows the theoretical I-V characteristics obtained using Eq. (17). The values of V_0 and I_0 are assumed to be temperature independent and the parameter α is determined at each temperature as the average of the two values obtained by fitting the height and width of the conductance peak. The parameter $V_0 = 73 \mu\text{V}$ is determined from ξ and u estimated in previous section, and I_0 is fitted to optimize the agreement between the theoretically calculated and experimentally measured height and width of the conductance peak at low temperatures⁶¹. The value of $I_0 = 4.9 \text{ pA}$ obtained by fitting the theory to

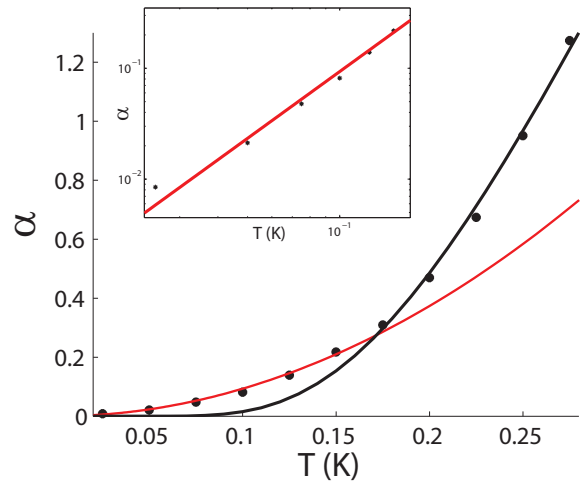


FIG. 6: (color online). Temperature dependence of α . The dots show the temperature dependence of α obtained by fitting the theoretical height and width of the conductance peak to the experimental results. The black and red lines are guides to the eye. The black line is an exponential curve $\alpha = c \cdot \exp(-T_0/T)$ ($c \approx 15.3$ and $T_0 \approx 0.69 \text{ K}$), where c and T_0 are fitted using the high-temperature ($T \geq 150 \text{ mK}$) experimental data. The red line shows $\alpha = (T/T_0)^2$ ($T_0 \approx 0.33 \text{ K}$), where T_0 is fitted using the low-temperature ($T \leq 125 \text{ mK}$) experimental data. Inset shows the temperature dependence of α at small temperatures plotted on a double logarithmic scale.

the experimental data is consistent with the estimate for $I_0 \sim 3.4 - 13.6 \text{ pA}$ (corresponding to $\Delta_{SAS} = 5 - 10 \mu\text{K}$ and $d/l_B = 1.5$) based on Eq. (16). The theoretically obtained I-V characteristics are in quantitative agreement with the experimental ones. In particular, as demonstrated in Fig. 5, we can quantitatively obtain the temperature dependencies of both the height and the width of the conductance peak by fitting a single parameter α at each temperature. Therefore, the approach outlined above is justified and we can concentrate on the temperature dependence of α , which is shown in Fig. 6. We can separate two regimes of temperatures, where the temperature dependence of α appears to be different from each other. As demonstrated in Fig. 6, at small temperatures it is conceivable that α obeys a power law, whereas at high-temperatures α shows thermally activated behavior $\alpha \propto e^{-T_0/T}$. These results seem to be in agreement with the expected temperature dependencies of the different physical processes possibly contributing to vortex field fluctuations^{14-16,19,20}. The large temperature behavior could be attributed to thermally activated hopping of merons whereas the power-law dependence could result from localized low-energy excitations¹⁴. Importantly, our analysis shows that as $T \rightarrow 0$ our parameter $\alpha \rightarrow 0$ indicating that $\tau_\varphi \rightarrow \infty$. (At lowest temperatures $\hbar/\tau_\varphi < k_B T$ and it is still decreasing reasonably rapidly with decreasing temperature.)

According to Eq. (4), the conductance diverges in the

limit $\tau_\varphi \rightarrow \infty$. Therefore, within our approach a diverging conductance at small temperatures is still expected by extrapolating the temperature dependence of α , which is consistent with the experimentally measured temperature dependencies of the height and width of the conductance peak. According to this analysis, the apparent temperature dependence $G_0 \propto \exp(-T/T_0)$ of the small-signal conductance arises because two different physical processes are contributing to the vortex field fluctuations at low and high temperatures, respectively.

We also point out that τ_φ can, in principle, be determined experimentally using a time-dependent interlayer voltage. Similarly to the case of Josephson junctions in the presence of strong fluctuations⁶², we expect that an ac field induces structures in the I-V characteristic at the resonances $eV \approx n\hbar\omega$ ($n = 1, 2, \dots$). These resonant structures resemble the Shapiro steps, but they are distinct from each other only if the frequency of the ac field satisfies $\omega > 1/\tau_\varphi$, allowing independent determination of τ_φ at different temperatures. Alternatively τ_φ could be determined by measuring the frequency dependence of the dynamical conductivity. At the smallest temperatures the required frequencies of the ac field are in the GHz frequency range.

IV. QUALITATIVE CHANGES CAUSED BY LARGER TUNNELING AMPLITUDE

We next study the effects caused by a larger tunneling amplitude. In a series of recent tunneling experiments^{43–46} samples with otherwise similar parameters but significantly larger tunneling amplitudes were used. The tunneling amplitude can again be determined either by using the tunneling I-V characteristics in the absence of magnetic field or by solving the Schrödinger and Poisson equations self-consistently. The obtained values of Δ_{SAS} vary between 100 – 150 μK ^{44,63}. This good agreement between the values obtained using two different methods suggests that the estimates for Δ_{SAS} are reliable. In comparison with the experiments discussed in the previous section, the tunneling amplitude of the samples in these experiments is therefore approximately an order of magnitude larger. Based on the scaling law $I_0 \propto \Delta_{SAS}^2$, Eq. (16), we expect that the tunneling currents are approximately two orders of magnitude larger $I_0 \sim 0.5 - 1 \text{ nA}$ ⁶⁴. This kind of scaling is in agreement with the experimental observations^{43–46}. Moreover, it was observed in the experiments⁴⁴ that the tunneling current is still proportional to the area of the sample. These observations indicate that essentially the same fluctuations-dominated physics determines the tunneling I-V characteristics also in these experiments. On the other hand, there are several important qualitative differences, which are discussed below. These new effects arise because the tunneling resistance is no longer large compared to the other resistances in the system.

A. Tunneling geometry

Because I_0 is now two orders of magnitude larger than in the earlier experiments, we estimate that the tunnel resistance at low temperatures is comparable to the contact resistances and intralayer resistances R_{xx} and R_{xy} . Although the interlayer voltage $V(\vec{r})$ is no longer constant, we can still expect that it varies reasonably slowly in space. This means that we can describe the transport in this system by assuming that the local tunnel current density is $I(V(\vec{r}))/L^2$, where $V(\vec{r})$ is the local interlayer voltage and $I(V)$ is the current-voltage characteristic given by Eq. (17). The interlayer voltage $V(\vec{r})$ can now be calculated by assuming that the intralayer transport and counterflow currents are described by resistivity tensors obtained from the experiments^{30,31,35–38}. An effective transport theory under these assumptions can be formulated using the current continuity equation and appropriate boundary conditions, which are determined by the experimental geometry.

Here we do not attempt to explain quantitatively all the details of the experiments but instead we just want to qualitatively explain the main features observed in the I-V characteristics. The main effect of the inhomogeneities in $V(\vec{r})$ is that all the sharp features in the I-V characteristics become rounded and dependent on the locations of the voltage probes. In particular, it becomes difficult to determine the tunneling conductance at small voltages, because the tunneling resistance is small compared to the other resistances in the system and the observed values of the interlayer voltage can depend on the locations of voltage probes⁴⁵. Nevertheless, the temperature dependence of the peak tunneling current^{44,45} is similar to that observed in the earlier experiments (Section III B) and therefore we expect that the perturbative approach is at least approximately valid even at the lowest experimental temperatures. By keeping in mind the type of small modifications discussed above, we can mainly ignore the inhomogeneities in the analysis of the remaining effects caused by larger tunneling amplitude.

Figs. 7(a), (c) and (e) show the results of experimental measurements at $d/l_B = 1.42$ and $T < 20 \text{ mK}$, reported in Ref. 44. The I-V characteristic shown in Fig. 7(e) is qualitatively very similar to the I-V characteristics obtained for samples with smaller tunneling amplitude (see Fig. 4). The main difference to the earlier experiments is that there now exists jumps at particular values of the voltage. If we assume that the inhomogeneities are not important, the experimental geometry can be described with an effective circuit shown in the inset in Fig. 7 (b). This gives us a circuit equation

$$V_{2t} - RI = V(I), \quad (18)$$

where the $V(I)$ characteristic of the bilayer tunnel junction is obtained from Eq. (17) by solving the voltage V as a function of current I . The solutions of Eq. (18) are obtained by finding the intersections of $V(I)$ characteristic and the lines $V_{2t} - RI$. We assume that $\alpha = 0.01$ and

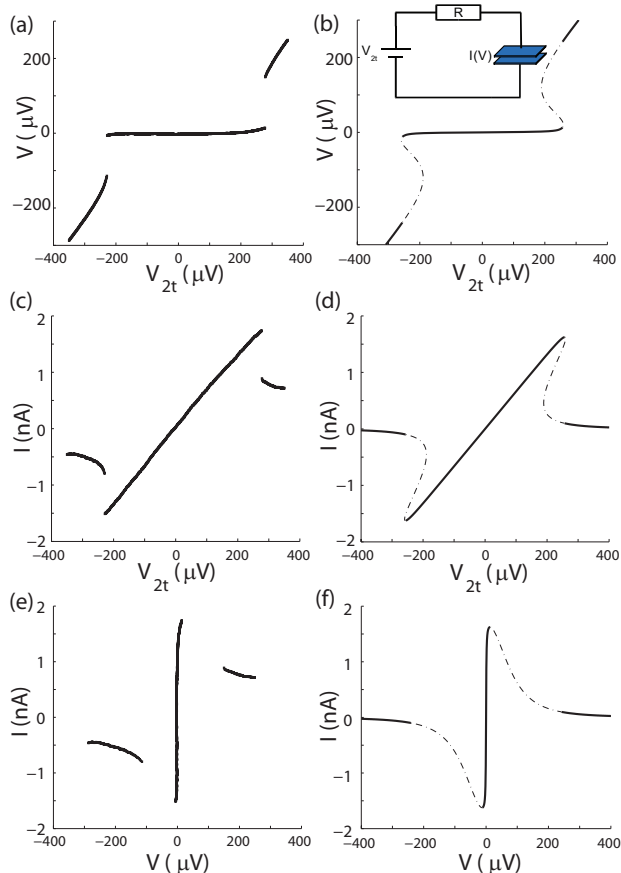


FIG. 7: (color online). (a),(c) Experimentally measured dependencies of the interlayer voltage V and the tunneling current I on the applied voltage V_{2t} . (e) Experimentally measured tunneling current I as a function of interlayer voltage V . The experimental measurements were made at $d/l_B = 1.42$ and $T < 20$ mK. (b), (d), (f) Corresponding theoretically calculated tunneling characteristics obtained using Eqs. (18) and (17). The theoretical parameters used in the calculation are $\alpha = 0.01$, $V_0 = 100 \mu\text{V}$ and $I_0 = 0.56$ nA. The inset in figure (b) shows the effective circuit. Resistance R is caused by the circuit and contact resistances. There exists a range of voltages V_{2t} , where Eq. (18) has several solutions. The additional solutions are indicated by the thin dashed lines in figures (b), (d) and (f). The experimental curves are reproduced from the experimental data provided by L. Tiemann *et al.* and reported in Refs. 44 and 45.

$V_0 = 100 \mu\text{V}$ in agreement with the values found in Section III. Because the effective resistance R is significantly larger than the tunneling resistance at small voltages, the resistance R can be determined from Fig. 7(c) by calculating the slope of the $I(V_{2t})$ characteristic at small applied voltages V_{2t} . We obtain $R \approx 150$ k Ω . Moreover, by fitting the theoretically calculated maximum of the tunneling current to the experimentally observed maximum current, we obtain $I_0 = 0.56$ nA. This value is in good agreement with an estimate $I_0 \sim 0.65$ nA obtained using Eq. (16) for $d = 28.6$ nm, $d/l_B = 1.4$, $L_x L_y = 880 \cdot 80 \mu\text{m}^2$, $\Delta_{SAS} = 100 \mu\text{K}$ and $\xi = 92$ nm (corresponding to

$V_0 = 100 \mu\text{K}$). Here we have assumed that u , ρ_s and Γ are the same as in the Caltech experiments. The results of the theoretical calculations for these values of α , R and I_0 are shown in Figs. 7 (b), (d) and (f). They are in good agreement with the experimental measurements. Moreover, we find that for particular values of V_{2t} , there exists several solutions of Eq. (18) indicating bistability. We expect that the jumps in the measured I-V characteristic [see Fig. 7 (e)] originate from a hysteretic switching caused by this bistability.

B. Counterflow geometry

Recently, tunneling experiments were performed also in the counterflow geometry [Fig. 8 (a)] using samples with similar $\Delta_{SAS} \sim 100 - 150 \mu\text{K}$.⁴⁶ In this case, dc input current is generated by applying a voltage to a large resistor in series with the system, and the current which passes through the top layer is redirected via a loop resistor into the bottom layer. If we assume that inhomogeneities are not playing an important role, we can construct an equivalent circuit shown in Fig. 8(b). The circuit equation is now

$$I_{\text{Total}} = I_{\text{Tunnel}} + I_{\text{Loop}} = I(V) + V/R, \quad (19)$$

where $I(V)$ is the tunneling I-V characteristic of the bilayer and R is an effective resistance, which takes into account the loop resistance R_L and the contact resistances.

Two intriguing observations were made in the experiment reported in Ref. 46. It was found that the tunneling current was large as long as the injected drive current was smaller than a certain critical current I_c at which point a transition into a new regime with negligible tunneling current was observed. For small d/l_B the observed transition is extremely sharp and becomes smoother for larger d/l_B as shown in Figs. 8 (c) and (d), respectively. Secondly, it was found that although the transition between the two tunneling regimes had only a minor impact on the state as observed in the magnetotransport, the longitudinal resistance increased rapidly for currents exceeding the critical current I_c . Our theory provides a simple and natural explanation for both experimental observations.

In order to explain these observations we assume that $\alpha = 0.01$ and $V_0 = 100 \mu\text{V}$ similar to the values used in previous sections. We determine $R = 180$ k Ω and $I_0 = 0.16$ nA ($d/l_B = 1.68$) and $I_0 = 0.48$ nA ($d/l_B = 1.37$) such that we visually obtain good agreement between theoretical and experimental dependencies of loop and tunneling current on the total current. The values of I_0 are in agreement with the measured tunneling currents at different d/l_B in the tunneling geometry^{44,45}. The effective resistance R is significantly larger than the loop resistance $R_L = 10$ k Ω used in the experiment⁴⁶, and therefore we expect that small variations in R_L would not affect the tunneling and loop currents significantly. Our calculations show that depending on the value of I_0

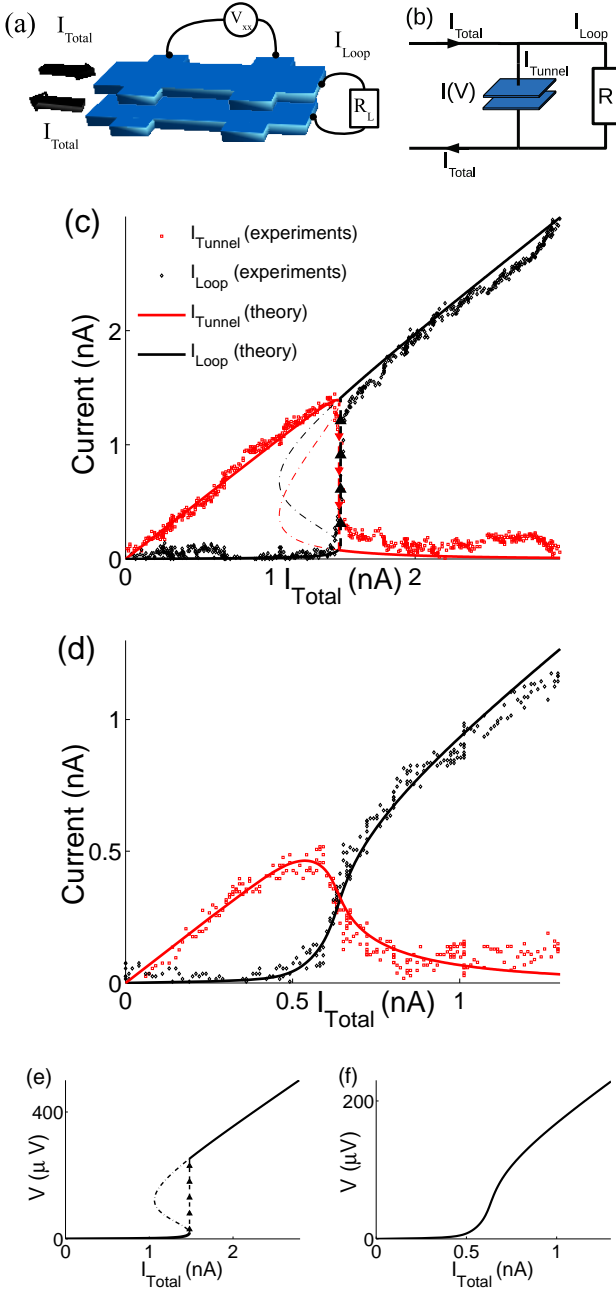


FIG. 8: (color online). (a) Counterflow geometry. (b) Equivalent circuit assuming homogeneous interlayer voltage. Here R is an effective resistance, which takes into account the loop resistance and contact resistances. (c), (d) Tunneling and loop currents as a function of total current. The experimental results shown in figures (c) and (d) are obtained for $d/l_B = 1.37$ and $d/l_B = 1.68$, respectively. In theoretical calculations we assume that R , α and V_0 are independent of d/l_B . The parameter I_0 is fitted to be $I_0 = 0.48$ nA and $I_0 = 0.16$ nA for the different values of $d/l_B = 1.37$ and $d/l_B = 1.68$, respectively. (e), (f) Interlayer voltages corresponding to the parameters used in figures (c) and (d), respectively. For $I_0 = 0.48$ nA there exist an interval of I_{Total} , where the Eq. (19) has several solutions. The additional solutions are shown by the thin dashed lines in figures (c) and (e). The experimental curves are reproduced from the experimental data provided by Y. Yoon *et al.* and reported in Ref. 46.

there exist two qualitatively different behaviors similarly to the ones observed in experiments. By inspecting the tunneling I-V characteristics (Figs. 4 and 7), we see that after the peak tunneling current has been reached the tunneling current decreases quickly with increasing voltage. If I_0/V_0 is large enough this decrease is more rapid than the increase of the loop current through the resistor. In this case, there exist several solutions of Eq. (19) around the critical current as demonstrated with the help of dashed lines in Figs. 8 (c), (e). We expect that this results in bistability, which can be seen as abrupt changes in the tunneling and loop currents in the experiments at small d/l_B . At large d/l_B the ratio I_0/V_0 is expected to be smaller and therefore the change in the tunneling and loop currents becomes smoother near the critical current. Our theoretical picture explains naturally why the transition has only a minor impact on the $\nu_T = 1$ state as observed in magnetotransport⁴⁶. The reason is simply that the transition occurs due to the tunneling I-V characteristic, which is an intrinsic property of the $\nu_T = 1$ state, and therefore in the first approximation it should have no effect at all on the $\nu_T = 1$ state. Moreover, according to our theory it is natural that the critical current observed in this counterflow geometry is almost exactly the same as the peak tunneling current observed in the tunneling geometry.

As already pointed out, the experiments also indicate that the dissipation increases rapidly at the currents exceeding the critical current. It has been suggested⁴⁶ that the increase of dissipation could be caused either by merons^{14–16,19,20} or so-called Josephson vortices²¹. However, the Josephson vortices could only exist if the Josephson length $\lambda_J = \sqrt{4\pi l_B^2 \rho_s / \Delta_{SAS}}$ was smaller or at least comparable to the coherence length ξ . This is not the case in the present experiments where we estimate $\lambda_J \sim 4$ μm . Moreover, the existence of Josephson vortices would indicate significantly larger critical currents²¹ than observed in the experiments. Therefore we expect that merons are responsible for the increased dissipation.

In our theoretical picture, the increase of dissipation should be due to a change in the dynamics of merons, which can be due to either an abrupt change in interlayer voltage or due to large counterflow current. If the effect was caused by the counterflow current it seems difficult to understand why the critical current is almost exactly equal to the maximum current observed in the tunneling geometry. Moreover, by assuming that the counterflow current induces a Magnus force on merons¹⁶ and that merons are confined into potential wells corresponding to the measured thermal activation gap³⁸, we estimate that the critical counterflow current necessary to depin the merons is significantly larger than typical experimental currents. On the other hand, we find that for small d/l_B the interlayer voltage significantly increases at the critical value of total current. Moreover, for both values of d/l_B , the interlayer voltage increases rapidly with increasing total current for currents exceeding the critical current [Figs. 8 (e), (f)], resembling the experimen-

tally observed dependence of the dissipation on the total current⁴⁶. Therefore, we believe that the increasing dissipation is tightly connected with the increasing interlayer voltage. By using our estimate for the exchange enhanced capacitance Γ , we find that an interlayer voltage of 100 μV can result in a density imbalance of several percents. It has been experimentally observed³⁸ and theoretically explained¹⁹ that such a density imbalance can significantly affect the longitudinal resistance. Furthermore, it is possible to experimentally test this hypothesis, because the density imbalance would result in different longitudinal resistances in the upper and lower layers^{19,38}.

V. RELATION TO PREVIOUS THEORETICAL APPROACHES

The theoretical explanation of charge transport in bilayer quantum Hall systems has been a long-standing theoretical problem. Perhaps most surprisingly, instead of a true Josephson effect, a Josephson-like conductance peak has been observed experimentally. Understanding the finite height and width of this small bias conductance peak and the calculation of critical tunneling currents has attracted a significant amount of interest. Theoretical approaches differ in whether they take a clean or a disordered system as a starting point of their analysis.

In the clean limit, the critical current is determined as the maximum current for which the pseudospin field can be static, and the dynamics of charge transfer between leads and bulk by quasi-particles plays an important role. Conductance peak heights and maximum tunnel currents predicted in the clean limit are orders of magnitude larger than the values observed in experiments,²³ and also differ from experiments with respect to the parametric dependencies of conductance peak and maximum tunnel current on sample area, bare tunneling amplitude, and in-plane magnetic field. Most notably, the critical tunnel current depends linearly or sublinearly on the tunneling amplitude Δ_{SAS} , and is independent of system size for systems larger than the Josephson length λ_J . In contrast, experiments seem to be consistent with a critical tunnel current proportional to both the area of the sample and to the square of the tunneling amplitude.

The influence of quenched disorder can be described by the introduction of a vortex field, which causes an exponential decay of pseudospin correlations with a characteristic spatial correlation length ξ . Under the assumption of a static vortex field, local pseudospin correlations are assumed to have an infinite range in time. One-dimensional numerical simulations indicate that the static vortex field results in an intriguing self-organized Bean critical state, where the current injected at the boundaries can affect the condensate dynamics throughout the whole sample.²⁴ By generalizing this finding to two-dimensional system, the authors in Refs. 24 and 25 find that if the sample size is sufficiently large, the critical tunneling current is proportional to the area of the

sample. This statement can be justified with the help of an energy optimization argument in the presence of random static vortex field^{24,25}, and it turns out that the sample size should be compared to a length scale λ_J^2/ξ . In the experiments reported in Ref. 44 the conditions $L_x, L_y > \lambda_J^2/\xi$ are approximately satisfied and the critical tunneling current proportional to the area of the sample has been observed. On the other hand, the approach based on the assumption of a static vortex field does not easily explain why a similar scaling with the area has been observed⁴⁰ also in samples, where the sample size is not large enough in comparison to the Josephson length. Other challenges for this type of approach are the explanations of the experimentally observed temperature and parallel magnetic field dependencies of the tunneling current, and the quantitative description of the height and width of the conductance peak. Nevertheless, one would expect that the vortex field should be static in the limit of zero temperature, and that the predictions of Refs. 24 and 25 should describe the limit of extremely low temperatures, which probably has not yet been reached experimentally.

Effects of a dynamical vortex field were analyzed in Refs. 10 and 11. In the present manuscript, we follow the approach outlined in Ref. 10, introduce a phenomenological vortex field, and calculate the dependence of experimental observables on the correlation length ξ and the correlation time τ_φ of the vortex field. We argue that all the important temperature dependence of experimental observables originates in the temperature dependence of the dimensionless decoherence rate $\alpha(T) = \xi/(u\tau_\varphi(T))$, and we determine $\alpha(T)$ by fitting experimental curves. The dynamics of merons was explored in Ref. 14 by means of mapping the quantum Hall bilayer to a classical two-dimensional XY model with a symmetry-breaking field and with disorder. It appears that disorder nucleates strings of overturned spins, which connect vortices and antivortices at their ends. At low temperatures, this state is characterized by anomalously large fluctuations of the vortex field, which are reminiscent of glassy dynamics. We believe that the power law like, weak temperature dependence of α which we extract from experiment may be consistent with the results of Ref. 14.

VI. DISCUSSION AND CONCLUSIONS

In this paper we have studied how the Josephson-like tunneling depends on the area and tunneling amplitude of the samples, applied parallel magnetic field and temperature. We have compared different theoretical approaches describing the Josephson-like tunneling and found that all the tunneling experiments are in agreement with a theory which treats fluctuations due to meron excitations phenomenologically and takes tunneling into account perturbatively. Previously, Josephson-like tunneling in samples with smaller^{28,29,32-34,39-42} and larger⁴³⁻⁴⁶ tunneling amplitudes have often been discussed in differ-

ent terms, because two orders of magnitude larger tunneling currents are found in latter experiments. Nevertheless, our analysis shows that all these experiments can be discussed within a common framework, and the observed magnitudes of the tunneling currents are in good agreement with the theory. We have also shown that the somewhat surprising temperature and in-plane magnetic field dependencies of tunneling current can be explained quantitatively by describing the effects caused by the merons with the help of a phenomenological vortex field. In this paper, we have concentrated on the description of the tunneling deep inside the coherent phase allowing us to make several simplifying approximations in Section II. However, we note that in principle the equations (10), (11), (12) and (9) could also be used to describe the Josephson-like tunneling closer to the phase-boundary separating the coherent and incoherent phases. This would allow the determination of the theoretical parameters of the model as a function of different experimentally controllable quantities such as d/l_B , density imbalance and temperature.

The surprisingly good agreement found between the theory and experiments naturally introduces several new theoretical questions. The temperature dependence of the tunneling currents was explained by fitting the parameter τ_φ , which describes the dynamics of the vortex field. However, the details related to the microscopic origin of the vortex field dynamics are not well-understood. The exponential temperature dependence at large temperatures most likely results from the thermally activated hopping of the merons, but the mechanism giving rise to the power law dependence at low temperatures requires additional theoretical analysis. Other interesting questions are related to the validity of the main approximation in our approach, which is the treatment of the tunneling as a perturbation. In general, the validity of this approximation depends on the nature of vortex-field fluctuations and dissipation mechanisms. We do not try to specify the dissipation processes here. Instead we expect on general grounds that the perturbative approach is controlled by a condition

$$\frac{L_i^2}{L^2} \frac{I(V)}{V} \ll \frac{e^2}{h}, \quad (20)$$

where L_i^2 defines the size of a domain which is large enough such that its dynamics can be considered to be independent of the other domains. The idea behind this inequality is that the left side defines the conductance of an independent domain and we interpret it as a transmission probability multiplying e^2/h . If the condition (20) is satisfied, the transmission probability is much smaller than one and the higher order tunneling processes are suppressed by the powers of the transmission probability. There are two relevant length scales, ξ and $u\tau_\varphi$, in the problem, which could determine the size of the independent domain L_i . Because at low temperatures $u\tau_\varphi \gg \xi$, the assumption $L_i^2 \approx (u\tau_\varphi)^2$ certainly yields the sufficient

condition

$$\frac{\xi^4}{\lambda_j^4} \frac{\rho_s}{\hbar/\tau_\varphi} \frac{\pi e^{-D_0/2}}{\alpha^2} \ll 1 \quad (21)$$

for the applicability of perturbation theory. In Appendix B, we obtain another condition (B15) for the validity of the perturbative approach in terms of the dissipation strength γ . For dimensional reasons, we expect that $\gamma u^2 \propto 1/\tau_\varphi^2$ so that the only possible difference between conditions (21) and (B15) is the reasonably large prefactor $\rho_s/(\hbar/\tau_\varphi)$ appearing in condition (21). This prefactor essentially originates from our assumption for the area L_i^2 of the independent domains. The result of the classical calculation in Appendix B can be interpreted as suggesting that the area for independent domains should be chosen as $L_i^2 \approx u\tau_\varphi\xi$, giving a less restrictive criterion for the applicability of perturbation theory.

Because the assumption used to obtain Eq. (21) likely overestimates L_i , we consider the condition (21) as a sufficient condition for the validity of the perturbative treatment of the tunneling, and we are confident that if it is satisfied, the perturbative approach is well justified. We find that the condition (21) is always satisfied in the experiments with smaller tunneling amplitude. In the case of larger tunneling amplitude, assuming that the temperature dependence of α does not change, this condition could break down (depending on the exact values of different theoretical parameters) at the smallest experimental temperatures. The experimental observation⁴³⁻⁴⁶ that there is no clear transition to a different operation regime as a function of temperature could indicate that the necessary condition for the perturbative treatment of tunneling is less restrictive than the condition (21) or that the larger tunneling currents resulted in an increase of the dissipation and the fluctuations. Experiments with even larger Δ_{SAS} could reveal this type of transition.

In this paper, we have discussed the Josephson-like tunneling at small voltages, where the theory and experiments are in good quantitative agreement with each other. On the other hand, it is clear (see Figs. 1 and 4) that our theoretical predictions differ from the experimental results at larger voltages. This discrepancy could be caused by the higher order terms in the Hamiltonian [Eq. (5)], a slightly incorrect form of the vortex field correlation function [Eq. (9)], the effects caused by the dissipation (see Appendix B) or an incoherent tunneling occurring inside compressible puddles of the electron liquid²⁰. The last possibility is supported by the experimental observation that at significantly larger voltages the tunneling I-V characteristic starts to look more and more similar to the corresponding I-V characteristic in the incoherent phase^{32,34}. Theoretical treatment of the tunneling at large voltages goes beyond the scope of the present paper.

Acknowledgments

We are indebted to A. Stern for important discussions and for guiding us through the literature on quantum Hall bilayers. We would like to acknowledge valuable discussions with W. Dietsche, J.P. Eisenstein, X. Huang, K. von Klitzing, J. Smet, E. Thuneberg, Y. Yoon and D. Zhang, and thank T. Wright for a critical reading of the manuscript. We thank J.P. Eisenstein and I.B. Spielman for providing the data used in figures 1, 2, 3, 4, 5, and W. Dietsche, L. Tiemann, Y. Yoon for providing the experimental data used in figures 7 and 8. This work was supported by the BMBF (German Ministry of Education and Research) Grant No. 01BM0900. B.R. would like to acknowledge the hospitality of the Aspen Center for Physics, where part of this work was done.

Appendix A: Calculation of the I-V characteristics

Similarly as in Josephson junctions⁵⁸ we can use Fermi's golden rule to calculate a forward tunneling rate

$$\vec{\Gamma}(V, B) = \frac{\lambda^2}{\hbar^2} \int_{-\infty}^{\infty} dt \int d^2 r_1 \int d^2 r_2 e^{ieVt/\hbar} e^{iQ_B(x_1-x_2)} \times \langle e^{i\varphi(\vec{r}_1, t)} e^{i\varphi_m(\vec{r}_1, t)} e^{-i\varphi(\vec{r}_2, 0)} e^{-i\varphi_m(\vec{r}_2, 0)} \rangle. \quad (\text{A1})$$

Due to the symmetry of the problem the backward tunneling rate is related to the forward tunneling rate as

$$\overleftarrow{\Gamma}(V, B) = \vec{\Gamma}(-V, -B). \quad (\text{A2})$$

By assuming that φ and φ_m commute, we get

$$I = e[\vec{\Gamma}(V, B) - \overleftarrow{\Gamma}(V, B)] = \frac{2\pi e \lambda^2 L^2}{\hbar} [S(Q_B, eV) - S(-Q_B, -eV)], \quad (\text{A3})$$

where

$$S(Q_B, eV) = \frac{1}{2\pi\hbar} \int_{-\infty}^{\infty} dt \int d^2 r e^{ieVt/\hbar} e^{iQ_B x} \times \langle e^{i\varphi(\vec{r}, t)} e^{-i\varphi(\vec{0}, 0)} \rangle G_m(r, t). \quad (\text{A4})$$

and

$$G_m(r, t) = \langle e^{i\varphi_m(\vec{r}, t)} e^{-i\varphi_m(\vec{0}, 0)} \rangle. \quad (\text{A5})$$

By defining the Fourier components of the operator fields φ and π as

$$\varphi_{\vec{k}} = \frac{1}{L} \int d^2 r e^{-i\vec{k}\cdot\vec{r}} \varphi(\vec{r}, t) \quad (\text{A6})$$

$$\pi_{\vec{k}} = \frac{1}{L} \int d^2 r e^{i\vec{k}\cdot\vec{r}} \pi(\vec{r}, t), \quad (\text{A7})$$

the commutation relations are $[\pi_{\vec{k}}, \varphi_{\vec{k}'}] = -i\hbar\delta_{\vec{k}, \vec{k}'}$, and the Hamiltonian defined by Eq. (5) can be rewritten as

$$H = \int d^2 r \mathcal{H} = \frac{\pi_0^2}{2M} + \sum_{\vec{k} \neq 0} \left[\frac{\pi_{\vec{k}} \pi_{-\vec{k}}}{2M} + \frac{M\omega_{\vec{k}}^2}{2} \varphi_{\vec{k}} \varphi_{-\vec{k}} \right], \quad (\text{A8})$$

where $M = \hbar^2 \Gamma / e^2$ and $\omega_{\vec{k}}$ is the dispersion relation for the collective Goldstone mode given by Eqs. (6) and (7).

The creation and annihilation operators $a_{\vec{k}}$ and $a_{\vec{k}}^\dagger$ are defined as

$$a_{\vec{k}} = \sqrt{\frac{M\omega_{\vec{k}}}{2\hbar}} \left(\varphi_{\vec{k}} + \frac{i}{M\omega_{\vec{k}}} \pi_{-\vec{k}} \right) \\ a_{\vec{k}}^\dagger = \sqrt{\frac{M\omega_{\vec{k}}}{2\hbar}} \left(\varphi_{-\vec{k}} - \frac{i}{M\omega_{\vec{k}}} \pi_{\vec{k}} \right). \quad (\text{A9})$$

It is easy to show that they satisfy commutation relations $[a_{\vec{k}}, a_{\vec{k}'}^\dagger] = \delta_{\vec{k}, \vec{k}'}$, $[a_{\vec{k}}^\dagger, a_{\vec{k}'}^\dagger] = 0$, $[a_{\vec{k}}, a_{\vec{k}'}] = 0$ and allow to rewrite the Hamiltonian as

$$H = \frac{\pi_0^2}{2M} + \sum_{\vec{k} \neq 0} \hbar\omega_{\vec{k}} \left(a_{\vec{k}}^\dagger a_{\vec{k}} + 1/2 \right). \quad (\text{A10})$$

We can now express $\varphi(\vec{r}, t)$ as a Fourier series

$$\varphi(\vec{r}, t) = \frac{1}{L} \varphi_0(t) + \frac{1}{L} \sum \left(\varphi_{\vec{k}}(t) e^{i\vec{k}\cdot\vec{r}} + \varphi_{-\vec{k}}(t) e^{-i\vec{k}\cdot\vec{r}} \right), \quad (\text{A11})$$

where the summation is taken so that each pair $\pm\vec{k}$ is counted only once. Thus the correlation function can be written as

$$\langle e^{i\varphi(\vec{r}, t)} e^{-i\varphi(\vec{0}, 0)} \rangle = \langle e^{\frac{i}{L} \varphi_0(t)} e^{-\frac{i}{L} \varphi_0(0)} \rangle \\ \times \prod \langle e^{\frac{i}{L} [\varphi_{\vec{k}}(t) e^{i\vec{k}\cdot\vec{r}} + \varphi_{-\vec{k}}(t) e^{-i\vec{k}\cdot\vec{r}}]} e^{-\frac{i}{L} [\varphi_{\vec{k}}(0) + \varphi_{-\vec{k}}(0)]} \rangle, \quad (\text{A12})$$

where the product is taken similarly over the pairs $\pm\vec{k}$ to avoid double counting.

By using the Baker-Hausdorff relation, we can rewrite Eq. (A12) as

$$\langle e^{i\varphi(\vec{r}, t)} e^{-i\varphi(\vec{0}, 0)} \rangle = e^{-iC(\vec{r}, t)/2} \langle e^{\frac{i}{L} [\varphi_0(t) - \varphi_0(0)]} \rangle \\ \times \prod \langle e^{\frac{i}{L} [\varphi_{\vec{k}}(t) e^{i\vec{k}\cdot\vec{r}} + \varphi_{-\vec{k}}(t) e^{-i\vec{k}\cdot\vec{r}} - \varphi_{\vec{k}}(0) - \varphi_{-\vec{k}}(0)]} \rangle, \quad (\text{A13})$$

where

$$C(\vec{r}, t) = \frac{i}{L^2} \left\{ [\varphi_0(t), \varphi_0(0)] \right. \\ \left. + \sum [\varphi_{\vec{k}}(t) e^{i\vec{k}\cdot\vec{r}} + \varphi_{-\vec{k}}(t) e^{-i\vec{k}\cdot\vec{r}}, \varphi_{\vec{k}}(0) + \varphi_{-\vec{k}}(0)] \right\}. \quad (\text{A14})$$

By using the Wick theorem for equilibrium correlation functions, it is easy to show that an operator ψ , which is a linear combination of creation and annihilation operators, satisfies

$$\frac{d}{d\alpha}\langle e^{i\alpha\psi}\rangle = -\alpha\langle\psi^2\rangle\langle e^{i\alpha\psi}\rangle, \quad (\text{A15})$$

and therefore $\langle e^{i\psi}\rangle = e^{-\frac{1}{2}\langle\psi^2\rangle}$.

By applying this result to Eq. (A13), we can rewrite the correlation function as

$$\langle e^{i\varphi(\vec{r},t)} e^{-i\varphi(0,0)}\rangle = e^{-iC(\vec{r},t)/2} e^{-D(\vec{r},t)/2}, \quad (\text{A16})$$

where

$$D(\vec{r},t) = \frac{t^2}{\beta ML^2} + \frac{1}{L^2} \left\{ \sum \langle [\varphi_{\vec{k}}(t)e^{i\vec{k}\cdot\vec{r}} + \varphi_{-\vec{k}}(t)e^{-i\vec{k}\cdot\vec{r}} - \varphi_{\vec{k}}(0) - \varphi_{-\vec{k}}(0)]^2 \rangle \right\}. \quad (\text{A17})$$

The functions C and D can now be calculated by expressing $\varphi_{\vec{k}}$ in terms of creation and annihilation operators. After a straightforward calculation, we obtain

$$\begin{aligned} C(\vec{r},t) &= \frac{1}{L^2} \left\{ \frac{e^2 t}{\hbar\Gamma} + \sum \frac{2u\hbar}{\rho_s k} \sin(\omega_{\vec{k}} t) \cos(\vec{k}\cdot\vec{r}) \right\} \\ &= \frac{1}{L^2} \left\{ \frac{e^2 t}{\hbar\Gamma} + \sum_{\vec{k}\neq 0} \frac{u\hbar}{\rho_s k} \sin(\omega_{\vec{k}} t) \cos(\vec{k}\cdot\vec{r}) \right\} \\ &= \frac{\hbar u}{L^2 \rho_s} \sum_{\vec{k}} \frac{1}{k} \sin(\omega_{\vec{k}} t) \cos(\vec{k}\cdot\vec{r}). \end{aligned} \quad (\text{A18})$$

Note that in each step we have changed the summation convention, so that finally the summation is over all \vec{k} vectors. In the final form the term corresponding to $\vec{k} = 0$ should be understood as a limit $k \rightarrow 0$ for the given expression.

It is easy to show that C is independent on the direction in the x,y-plane $C(\vec{r},t) = C(r,t)$ and that $C(r,-t) = -C(r,t)$. Moreover, for $t > 0$

$$C(r,t) = \frac{\hbar}{2\pi\rho_s} \theta(ut-r) \frac{1}{\sqrt{t^2 - (\frac{r}{u})^2}}. \quad (\text{A19})$$

The last expression is easiest to prove by calculating the Fourier expansion for the right side of Eq. (A19).

Similarly, we get

$$D(\vec{r},t) = \sum_{\vec{k}} \frac{\hbar u}{L^2 \rho_s k} [1 - \cos(\omega_{\vec{k}} t) \cos(\vec{k}\cdot\vec{r})] \coth(\beta\hbar\omega_{\vec{k}}/2), \quad (\text{A20})$$

where the $\vec{k} = 0$ term should be calculated by setting $\cos(\vec{k}\cdot\vec{r}) \rightarrow 1$ and taking the limit $k \rightarrow 0$ for the rest of the expression. It is again easy to show that $D(\vec{r},t) = D(r,t)$ and $D(r,-t) = D(r,t)$.

By using Eqs. (A3), (A4) and (A16) and the properties $C(\vec{r},t) = C(r,t)$, $D(\vec{r},t) = D(r,t)$, $C(r,-t) = -C(r,t)$, $D(r,-t) = D(r,t)$ and $G_m(r,-t) = G_m(r,t)$, we get equations (10), (11) and (12).

Appendix B: Derivation of the I-V characteristics using Sine-Gordon equation

The Lagrangian density corresponding to Hamiltonian density (5) is

$$\mathcal{L} = \frac{\hbar^2\Gamma}{2e^2} \dot{\varphi}^2 - \frac{\rho_s}{2} (\nabla\varphi)^2 + 2\lambda \cos \left[\varphi + \varphi_m + Q_B x + \frac{eVt}{\hbar} \right]. \quad (\text{B1})$$

The equation of motion for φ can be written as a Sine-Gordon equation

$$\nabla^2\varphi - \frac{1}{u^2} \partial_t^2\varphi - \hat{\gamma}\varphi = \frac{1}{\lambda_J^2} \sin \left[\varphi + \varphi_m + Q_B x + eVt/\hbar \right], \quad (\text{B2})$$

where we have introduced an operator $\hat{\gamma}$, which describes the dissipative terms in our model. The actual mechanism of the dissipation is not well-understood, but several different dissipative terms have been proposed^{12,21,23}. Here we keep the dissipative terms unspecified for as long as possible.

The idea is to formulate the perturbative tunneling theory so that we would only need to assume that the variations of φ are small within certain reasonably large space and time scales. More concretely, we divide the space-time into domains (labeled with index i) of size T_i (time-interval) and L_i^2 (spatial area). We denote the average value of φ inside the domains as $\bar{\varphi}_i$, and assume that the variations within the domain are small, $\delta\varphi_i(\vec{r}_i, t_i) = \varphi(\vec{r}_i, t_i) - \bar{\varphi}_i \ll 1$. The variations $\delta\varphi_i$ inside each domain i are not entirely independent on the other domains because the domains can be dynamically coupled with each other. Here we assume that the domains are large enough that the boundary conditions are not important. Although the boundary conditions strongly affect the state of the whole system in the case of static vortex field²⁴, we believe that our approximation can be justified in the typical experimental situation where the fluctuations of the vortex field are important.

Inside each space-time domain we need to solve an equation

$$\nabla^2\delta\varphi_i - \frac{\partial_t^2\delta\varphi_i}{u^2} - \hat{\gamma}\delta\varphi_i = \frac{1}{\lambda_J^2} \sin \left[\bar{\varphi}_i + \varphi_m + Q_B x + \frac{eVt}{\hbar} \right]. \quad (\text{B3})$$

The time average of tunneling current $I(V)$ can then be calculated from equation

$$\begin{aligned} \langle I(V) \rangle &= \frac{e}{\hbar} \frac{\Delta_{SAS}}{4\pi l_B^2} \sum_i \frac{1}{T_i} \int dt_i \int d^2 r_i \\ &\times \langle \sin [\delta\varphi_i(\vec{r}_i, t_i) + \bar{\varphi}_i + \varphi_m(\vec{r}_i, t_i) + Q_B x_i + eVt_i/\hbar] \rangle. \end{aligned} \quad (\text{B4})$$

Here $\sum_i T_i \rightarrow \infty$ is the total time, $\langle \dots \rangle$ denotes the ensemble average over different realizations of the vortex field and the integrations are over the space-time domains.

It is easy to show that a particular solution of Eq. (B3) can be written as

$$\delta\varphi_i(\vec{r}_i, t_i) = C_i + \frac{1}{\lambda_J^2} \int \int d^2r' dt' G(\vec{r}_i - \vec{r}', t_i - t') \times \sin \left[\bar{\varphi}_i + \varphi_m(\vec{r}', t') + Q_B x' + eVt'/\hbar \right], \quad (\text{B5})$$

where

$$G(\vec{r}, t) = \frac{1}{L^2} \frac{1}{2\pi} \sum_{\vec{k}} \int d\omega G(\vec{k}, \omega) e^{i\vec{k}\cdot\vec{r}} e^{-i\omega t},$$

$$G(\vec{k}, \omega) = \frac{1}{-k^2 + \frac{\omega^2}{u^2} + i\gamma(\omega, \vec{k})} \quad (\text{B6})$$

and

$$C_i = -\frac{1}{T_i L_i^2} \int dt_i \int d^2r_i \frac{1}{\lambda_J^2} \int \int d^2r' dt' \times G(\vec{r}_i - \vec{r}', t_i - t') \sin \left[\bar{\varphi}_i + \varphi_m(\vec{r}', t') + Q_B x' + eVt'/\hbar \right] \quad (\text{B7})$$

is a constant guaranteeing that $\bar{\varphi}_i$ is the average value of φ within the domain i i.e.

$$\int dt_i \int d^2r_i \delta\varphi_i(\vec{r}_i, t_i) = 0. \quad (\text{B8})$$

We have also assumed that the dissipation operator acting on the plane waves satisfied the following equation

$$\hat{\gamma} e^{i\vec{k}\cdot\vec{r}} e^{-i\omega t} = -i\gamma(\omega, \vec{k}) e^{i\vec{k}\cdot\vec{r}} e^{-i\omega t}. \quad (\text{B9})$$

We assume that the dissipation is isotropic in the (x, y) -plane, $\gamma(\omega, \vec{k}) = \gamma(\omega, k)$. Moreover, we require that $G(-\omega, -\vec{k}) = G^*(\omega, \vec{k})$, which gives $\gamma(-\omega, k) = -\gamma(\omega, k)$.

By assuming that the instantaneous value of the vortex field $\varphi_m(\vec{r}, t)$ and the average quantities C_i and $\bar{\varphi}_i$ are statistically independent, we obtain using Eqs. (B4) and (B5) that the tunneling current $I(V)$ can be written as

$$\langle I(V) \rangle = \frac{1}{2} \frac{e \Delta_{SAS}}{\hbar} \frac{1}{4\pi l_B^2} \frac{1}{\lambda_J^2} \text{Im} \left\{ \sum_i \frac{1}{T_i} \int dt_i \int d^2r_i \int \int d^2r' dt' G(\vec{r}_i - \vec{r}', t_i - t') \times \left\langle e^{i[\varphi_m(\vec{r}', t') + Q_B x' + eVt'/\hbar - \varphi_m(\vec{r}_i, t) - Q_B x_i - eVt_i/\hbar]} \right\rangle \right\}. \quad (\text{B10})$$

Here we have taken into account that the vortex field tends to stay constant over some time and space interval and therefore the differences of the vortex field values $\varphi_m(\vec{r}', t') - \varphi_m(\vec{r}_i, t)$ are correlated. On the other

hand, the actual value of the vortex field $\varphi_m(\vec{r}, t)$ can be arbitrary, and therefore only the terms proportional to $e^{\pm i[\varphi_m(\vec{r}', t') - \varphi_m(\vec{r}_i, t)]}$ can contribute to the average current. Physically this means that the fluctuations of the vortex field destroy the supercurrent.

By assuming also that correlation function for the vortex field is given by Eq. (9), we obtain [$R = r/\xi$, $q = k\xi$, $\Omega = \omega\xi/u$, $\gamma'(\Omega, q) = \gamma(\Omega u/\xi, q/\xi)$]

$$\langle I \rangle = I'_0 \int_0^\infty dq \int_0^\infty d\Omega \left\{ \frac{\gamma'(\Omega, q)\xi^2}{(\Omega^2 - q^2)^2 + [\gamma'(\Omega, q)\xi^2]^2} \times \frac{2q}{\pi} \left[\frac{\alpha}{\alpha^2 + (-\Omega + V/V_0)^2} - \frac{\alpha}{\alpha^2 + (\Omega + V/V_0)^2} \right] \times \int dR Re^{-R} J_0(Q_B \xi R) J_0(qR) \right\}, \quad (\text{B11})$$

where V_0 and α are given by Eqs. (1) and (3), respectively. The current scale is now determined by

$$I'_0 = \frac{e \Delta_{SAS}}{\hbar} \frac{L^2 \xi^2}{16\pi l_B^2 \lambda_J^2} = \frac{e \xi^2 L^2 \Delta_{SAS}^2}{\hbar l_B^4 \rho_s} \frac{1}{64\pi^2}, \quad (\text{B12})$$

which differs from the expression (16) by a factor $e^{-D_0/2}$.

If we further assume that $\gamma'(\Omega, q)\xi^2 \ll 1$, we can use

$$\lim_{\epsilon \rightarrow 0} \frac{1}{\pi} \frac{\epsilon}{(y^2 - y_0^2)^2 + \epsilon^2} = \frac{1}{2|y_0|} [\delta(y + y_0) + \delta(y - y_0)] \quad (\text{B13})$$

to obtain

$$\langle I \rangle = I'_0 \int dq \left[\frac{\alpha}{\alpha^2 + (V/V_0 - q)^2} - \frac{\alpha}{\alpha^2 + (V/V_0 + q)^2} \right] \times \int dR Re^{-R} J_0(Q_B \xi R) J_0(qR). \quad (\text{B14})$$

The only difference to the expression (15) is that the current scale I_0 determined by Eq. (16) is now replaced by I'_0 given by Eq. (B12). We see from Eq. (B11) that in the general case also the dependence of the dissipation on the frequency and momentum of the pseudospin waves can affect the I-V characteristic.

In order to determine the limits of validity of the perturbation theory we need to calculate $\langle [\varphi(\vec{r}, t) - \varphi(\vec{0}, 0)]^2 \rangle = \langle [\delta\varphi(\vec{r}, t) - \delta\varphi(\vec{0}, 0)]^2 \rangle = 2\langle \delta\varphi^2(\vec{r}, t) \rangle - 2\langle \delta\varphi(\vec{r}, t)\delta\varphi(\vec{0}, 0) \rangle$. Using similar methods as above, we obtain that the perturbation theory is controlled by a condition

$$\frac{\xi^4}{\lambda_J^4} \frac{1}{\gamma \xi^2} \ll 1, \quad (\text{B15})$$

where for simplicity we have assumed that the dissipation γ does not depend on frequency and momentum.

-
- ¹ S. M. Girvin and A. H. MacDonald, *Perspectives in Quantum Hall effects*, edited by S. Das Sarma and A. Pinczuk (Wiley, New York, 1997), Chap V; J. P. Eisenstein, *ibid.*, Chap II.
- ² S. M. Girvin, The Quantum Hall Effect: Novel Excitations and Broken Symmetries, Proceedings of the Les Houches Summer School (Springer-Verlag, Berlin, 1999).
- ³ S. M. Girvin, Phys. Today **53**, 39 (2000).
- ⁴ J. P. Eisenstein and A. H. MacDonald, Nature **432**, 691 (2004).
- ⁵ T. Chakraborty and P. Pietiläinen, Phys. Rev. Lett. **59**, 2784 (1987).
- ⁶ H. A. Fertig, Phys. Rev. B **40**, 1087 (1989).
- ⁷ K. Yang *et al.*, Phys. Rev. Lett. **72**, 732 (1994); K. Moon *et al.*, Phys. Rev. B **51**, 5138 (1995); K. Yang *et al.*, Phys. Rev. B **54**, 11644 (1996).
- ⁸ X. G. Wen and A. Zee, Phys. Rev. B **47**, 2265 (1993); Z. F. Ezawa and A. Iwazaki, Phys. Rev. B **47**, 7295 (1993).
- ⁹ Z. F. Ezawa and A. Iwazaki, Int. J. Mod. Phys. B **8**, 2111 (1994).
- ¹⁰ A. Stern *et al.*, Phys. Rev. Lett. **86**, 1829 (2001).
- ¹¹ L. Balents and L. Radzihovsky, Phys. Rev. Lett. **86**, 1825 (2001).
- ¹² M. M. Fogler and F. Wilczek, Phys. Rev. Lett. **86**, 1833 (2001).
- ¹³ Y. N. Joglekar and A. H. MacDonald, Phys. Rev. Lett. **87**, 196802 (2001).
- ¹⁴ H. A. Fertig and J. P. Straley, Phys. Rev. Lett. **91**, 046806 (2003).
- ¹⁵ H. A. Fertig and G. Murthy, Phys. Rev. Lett. **95**, 156802 (2005); H. A. Fertig and G. Murthy, Solid State Commun. **140**, 83 (2006).
- ¹⁶ D. A. Huse, Phys. Rev. B **72**, 064514 (2005).
- ¹⁷ Z. Wang, Phys. Rev. Lett. **94**, 176804 (2005).
- ¹⁸ E. Rossi, A. S. Nunez and A. H. MacDonald, Phys. Rev. Lett. **95**, 266804 (2005).
- ¹⁹ B. Roostaei *et al.*, Phys. Rev. Lett. **101**, 046804 (2008).
- ²⁰ P. R. Eastham, N. R. Cooper and D. K. K. Lee, Phys. Rev. B **80**, 045302 (2009).
- ²¹ D. V. Fil and S. I. Shevchenko, J. Phys. Condens. Matter **21**, 215701 (2009).
- ²² J. Sun *et al.*, Phys. Rev. B **81**, 195314 (2010).
- ²³ J.-J. Su and A. H. MacDonald, Phys. Rev. B **81**, 184523 (2010).
- ²⁴ P. R. Eastham, N. R. Cooper and D. K. K. Lee, arXiv:1003.5191 (2010).
- ²⁵ D. K. K. Lee, P. R. Eastham and N. R. Cooper, arXiv:1011.3943 (2010).
- ²⁶ For a detailed discussion of the phase-transition, see Y. Zou *et al.*, Phys. Rev. B **81**, 205313 (2010) and references therein.
- ²⁷ S. Q. Murphy *et al.*, Phys. Rev. Lett. **72**, 728 (1994).
- ²⁸ I. B. Spielman *et al.*, Phys. Rev. Lett. **84**, 5808 (2000).
- ²⁹ I. B. Spielman *et al.*, Phys. Rev. Lett. **87**, 036803 (2001).
- ³⁰ M. Kellogg *et al.*, Phys. Rev. Lett. **88**, 126804 (2002).
- ³¹ M. Kellogg *et al.*, Phys. Rev. Lett. **90**, 246801 (2003).
- ³² J. P. Eisenstein, Solid State Commun. **127**, 123 (2003).
- ³³ I. B. Spielman *et al.*, Phys. Rev. B **70**, 081303 (2004).
- ³⁴ I. B. Spielman, Ph.D. thesis, Caltech (2004).
- ³⁵ M. Kellogg *et al.*, Phys. Rev. Lett. **93**, 036801 (2004).
- ³⁶ E. Tutuc, M. Shayegan and D. A. Huse, Phys. Rev. Lett. **93**, 036802 (2004).
- ³⁷ E. Tutuc and M. Shayegan, Phys. Rev. B **72**, 081307 (2005).
- ³⁸ R. D. Wiersma *et al.*, Phys. Rev. Lett. **93**, 266805 (2004); R. D. Wiersma *et al.*, Physica E **35**, 320 (2006).
- ³⁹ I. B. Spielman *et al.*, Phys. Rev. Lett. **94**, 076803 (2005).
- ⁴⁰ A. D. K. Finck *et al.*, Phys. Rev. B **78**, 075302 (2008).
- ⁴¹ A. R. Champagne *et al.*, Phys. Rev. Lett. **100**, 096801 (2008).
- ⁴² A. R. Champagne *et al.*, Phys. Rev. B **78**, 205310 (2008).
- ⁴³ L. Tiemann *et al.*, New. J. Phys. **10**, 045018 (2008).
- ⁴⁴ L. Tiemann *et al.*, Phys. Rev. B **80**, 165120 (2009).
- ⁴⁵ L. Tiemann, Ph. D. thesis, Stuttgart (2008).
- ⁴⁶ Y. Yoon *et al.*, Phys. Rev. Lett. **104**, 116802 (2010).
- ⁴⁷ P. Giudici *et al.*, Phys. Rev. Lett. **100**, 106803 (2008).
- ⁴⁸ A. D. K. Finck *et al.*, Phys. Rev. Lett. **104**, 016801 (2010).
- ⁴⁹ J. P. Eisenstein, L. N. Pfeiffer and K. W. West, Phys. Rev. Lett. **69**, 3804 (1992).
- ⁵⁰ J. P. Eisenstein, L. N. Pfeiffer and K. W. West, Phys. Rev. Lett. **74**, 1419 (1995).
- ⁵¹ K. M. Brown *et al.*, Phys. Rev. B **50**, 15465 (1994).
- ⁵² N. Turner *et al.*, Phys. Rev. B **54**, 10614 (1996).
- ⁵³ P. Johansson and J. M. Kinaret, Phys. Rev. Lett. **71**, 1435 (1993); Phys. Rev. B **50**, 4671 (1994).
- ⁵⁴ F. D. Klironomos and A. T. Dorsey, Phys. Rev. B **71**, 155331 (2005).
- ⁵⁵ A. Steinbach *et al.*, Phys. Rev. Lett. **87**, 137003 (2001).
- ⁵⁶ G.-L. Ingold, H. Grabert and U. Eberhardt, Phys. Rev. B **50**, 395 (1994); H. Grabert, G.-L. Ingold and B. Paul, Europhys. Lett. **44**, 360 (1998); G.-L. Ingold and H. Grabert, Phys. Rev. Lett. **83**, 3721 (1999).
- ⁵⁷ Yu. M. Ivanchenko and L. A. Zil'berman, Sov. Phys. JETP **28**, 1272 (1969); V. Ambegaokar and B. I. Halperin, Phys. Rev. Lett. **22**, 1364 (1969).
- ⁵⁸ G.-L. Ingold and Yu. V. Nazarov, in Single Charge Tunneling, edited by H. Grabert and M. H. Devoret, NATO ASI, Ser. B, Vol. 294 (Plenum, New York, 1992).
- ⁵⁹ S. Q. Murphy *et al.*, Phys. Rev. B **52**, 14825 (1995).
- ⁶⁰ M. Tinkham, Introduction to superconductivity, Second Edition, (Dover, New York, 2004), Section 6.4.
- ⁶¹ We vary I_0 and determine α for each temperature as the average of the two values obtained by fitting the height and width of the conductance peak. We choose the value for I_0 by minimizing a cost function $\sum [|\log(G_0(\alpha_i)/G_i)/\log(G_{\max}/G_{\min})| + |(V_{HWHM}(\alpha_i) - V_i)/V_0|]$, where the summation is over the five lowest temperatures, α_i are the values of α fitted at each temperature, $G_0(\alpha_i)$ and G_i are the theoretically calculated and experimentally measured peak conductances, G_{\max} and G_{\min} are the experimentally measured maximum and minimum peak conductances in the temperature interval $T = 25 - 300$ mK, and $V_{HWHM}(\alpha_i)$ and V_i are the theoretically calculated and experimentally measured half widths at half maximums for the conductance peaks.
- ⁶² Y. Koval, M. V. Fistul and A. V. Ustinov, Phys. Rev. Lett. **93**, 087004 (2004); G. Falci, V. Bubanja and G. Schön, Z. Phys. B **85**, 451 (1991).
- ⁶³ The experimental data used in the determination of the tunneling amplitude from the I-V characteristic at $B = 0$ was provided by L. Tiemann *et al.* and has been reported in Refs. 44 and 45.

⁶⁴ There are some sample to sample variations also in other parameters and therefore it is not meaningful to try to make the prediction for I_0 more accurate. However, we point out that it would be very useful to study experi-

mentally the scaling of I_0 as a function of Δ_{SAS} by using samples which have otherwise as identical parameters as possible.